Use of a Novel Arg-Gly-Asp Radioligand, ^{18}F-AH111585, to Determine Changes in Tumor Vascularity After Antitumor Therapy

Matthew S. Morrison[1], Sally-Ann Ricketts[2], Jon Barnett[1], Alan Cuthbertson[3], Jean Tessier[2], and Stephen R. Wedge[2]

[1]GE Healthcare MDx Research, The Grove Centre, Amersham, United Kingdom; [2]AstraZeneca, Alderley Park, Macclesfield, Cheshire, United Kingdom; and [3]GE Healthcare MDx Research, Nycoveien 2, Oslo, Norway

Despite the recent development of various radiolabeled Arg-Gly-Asp (RGD) peptides for imaging the $\alpha_v\beta_3$ integrin receptor, relatively little attention has been focused on the ability of these radiotracers to monitor changes in tumor vascularity after antitumor therapies. This study describes the favorable in vivo kinetics and tumor-targeting properties of ^{18}F-AH111585, a novel ^{18}F-RGD peptide, and its ability to monitor tumor vascularity noninvasively. **Methods:** Mice bearing Lewis lung carcinoma (LLC) tumors or Calu-6 non–small cell lung tumor xenografts were used for in vivo biodistribution and small-animal PET imaging studies. In addition, some animals were treated with either low-dose paclitaxel or the vascular endothelial growth factor receptor-2 tyrosine kinase inhibitor ZD4190. Tumor uptake of ^{18}F-AH111585 and microvessel density were then assessed. **Results:** Biodistribution of ^{18}F-AH111585 demonstrated rapid clearance from the blood and key background organs and good tumor accumulation, with 1.5 percentage injected dose per gram (%ID/g) present at 2 h after injection in LLC tumors. Small-animal PET imaging of Calu-6 tumors allowed visualization of tumors above background tissue, with mean baseline uptake of 2.2 %ID/g. Paclitaxel therapy reduced the microvessel density in LLC tumor–bearing mice and resulted in significantly reduced ^{18}F-AH111585 tumor uptake ($P < 0.05$). ZD4190 therapy resulted in a significant (31.8%) decrease in ^{18}F-AH111585 uptake in Calu-6 tumors, compared with the vehicle control–treated Calu-6 tumors, which had a 26.9% increase in ^{18}F-AH111585 uptake over the same period ($P < 0.01$). **Conclusion:** ^{18}F-AH111585 is a promising ^{18}F-labeled RGD tracer that offers a new approach to noninvasively image tumor vasculature. This tracer may reveal important information in the assessment of the impact of antitumor therapies, in particular those that predominantly target tumor blood vessels.

Key Words: RGD peptide; PET; integrin $\alpha_v\beta_3$; integrin $\alpha_v\beta_5$; tumor vasculature; molecular imaging

J Nucl Med 2009; 50:116–122
DOI: 10.2967/jnumed.108.056077

Received Jul. 17, 2008; revision accepted Oct. 8, 2008.
For correspondence or reprints contact: Matthew Morrison, GE Healthcare, The Grove Centre, White Lion Rd., Amersham, Bucks, HP7 9LL, U.K.
E-mail: matthew.morrison@ge.com

Several novel therapeutic strategies being examined clinically aim to modify tumor vasculature function, growth, and survival (*1*). These include the inhibition of vascular endothelial growth factor-A (VEGF) signaling (*1*) (a key regulator of tumor angiogenesis, vascular permeability, and neovascular survival), use of vascular disrupting agents (VDAs) such as the tubulin-depolymerising agent combretastatin A-4 (*2*), or examination of low-dose cytotoxic chemotherapy (*3*). To monitor the effect of VEGF-signaling inhibitors or VDAs, MRI and CT scans, and in particular dynamic contrast-enhanced MRI and CT, have been used successfully to provide evidence of an effect on tumor blood flow, blood volume, and permeability (*4,5*). However, an obvious current limitation to being able to understand the full activity of approaches that target the tumor vasculature is the lack of a noninvasive imaging method to quantify changes in tumor vascularity in patients with cancer (*6*). This may become of greater importance as alternative (i.e., non-VEGF or -VDA) therapies progress clinically (*1*), because these may have more subtle and less-predictable acute effects on tumor hemodynamics.

The purpose of this work was to assess preclinically the potential of a PET tracer (^{18}F-AH111585) currently in an early clinical trial. ^{18}F-AH111585 is an ^{18}F-radiolabeled small peptide containing an Arg-Gly-Asp (RGD) sequence, with binding affinities to $\alpha_v\beta_3$, $\alpha_v\beta_5$, and $\alpha_{iib}\beta_3$ integrins determined to be 11, 0.1, and 281 nM, respectively (*7*), indicating that the product has retained selective binding affinity to the receptors, compared with the original peptide sequence.

Integrins are composed of a family of heterodimeric glycoproteins involved in cell–cell and cell–matrix interactions (*8*). They consist of α and β subunits that form noncovalent $\alpha\beta$ heterodimers (*9*) and are the major receptors by which cells attach to the extracellular matrix. The $\alpha_v\beta_3$ integrin, which is preferentially expressed on proliferating endothelial cells associated with neovascularization in both malignant tumors and normal tissue, but not in quiescent blood vessels (*10,11*), has been identified as a target for

imaging neovasculature. Others have shown previously (*12–14*) that RGD peptides can serve as a targeting biomolecule to carry a range of radionuclides (e.g., ^{18}F, ^{99m}Tc, and ^{64}Cu) to the $\alpha_v\beta_3$ integrin. Thus, targeting the $\alpha_v\beta_3$ integrin receptor with ^{18}F-AH111585 could provide us with a tool to examine the effect of vascular-modulation therapies directly, without having to rely on consequential changes in blood perfusion and permeability. A method to analyze the effect of vascular-modulation therapies directly may be particularly pertinent to examining therapies that specifically target the tumor vasculature, given that their activity may not lead to a substantial tumor mass or volume reduction, particularly soon after therapy (*15,16*). Hence, conventional measurements of response may be insensitive or markedly delayed even when there is a significant therapeutic effect. Direct clinical imaging of tumor neovasculature could, therefore, provide the opportunity to optimize dose selection during early examination of a novel antivascular therapy.

The initial aim of this work was to determine the biodistribution of ^{18}F-AH111585 in tumor-bearing mice to establish the suitability of ^{18}F-AH111585 as an imaging agent for tumor vasculature. Subsequently, the effect of treatment with either low-dose paclitaxel or ZD4190, a small molecular VEGF receptor-2 (VEGFR-2) tyrosine kinase inhibitor (*17*), was examined using ^{18}F-AH111585 and small-animal PET imaging.

MATERIALS AND METHODS

Radiochemistry

The chemical synthesis of the precursor for ^{18}F-AH111585 has been described previously (*18*). Radiosynthesis was performed at GE Healthcare, The Grove Centre. A full description of the synthesis has been published elsewhere (*19*). Briefly, ^{18}F-fluoride was azeotropically dried in the presence of Kryptofix (K_{222}; Merck) (11 mg in 1.0 mL of acetonitrile) and potassium carbonate (1.4 mg in 1 mL of acetonitrile) by heating under a flow of nitrogen, followed by a vacuum for 15 min. Care was taken to ensure that all traces of acetonitrile were removed. The $K_{222}/K^+/F^-$ complex was cooled to less than 40°C, and AH111360 (3 mg in 1 mL of dimethyl sulfoxide) was added. The reaction vessel was sealed and heated to 90°C for 15 min to effect radiolabeling. The crude ^{18}F-*p*-fluorobenzaldeyde solution was then cooled to room temperature, diluted with water, and passed through a C18 solid-phase extraction cartridge in which ^{18}F-*p*-fluorobenzaldeyde was retained and excess precursor, K_{222}, dimethyl sulfoxide, and hydrophilic by-products were eluted to waste. ^{18}F-*p*-fluorobenzaldeyde was subsequently recovered in acetonitrile for conjugation with peptide. The peptide (AH111695) was dissolved in 0.1 M phosphate/citrate solution (pH 2.5; 1.0 mL) and combined with the purified ^{18}F-*p*-fluorobenzaldeyde solution in the reaction vessel. The vessel was sealed and heated to 70°C for 15 min to effect conjugation. After we cooled the crude conjugate to room temperature, it was purified by preparative high-performance liquid chromatography. The product fraction was formulated with phosphate-buffered saline (pH 7).

The radiochemical purity of the injectate determined by high-performance liquid chromatography was greater than 95%.

Preparation of Tumor-Bearing Mice

All animal studies were approved by and performed in compliance with the U.K. Home Office guidelines. Two types of tumor models were used for the in vivo biodistribution and imaging studies, both with known low levels of tumor-cell $\alpha_v\beta_3$ expression. Lewis lung carcinoma (LLC) cells (American Type Culture Collection) derived from mouse lung cancer were maintained in Dulbecco's modified Eagle medium (Sigma-Aldrich). Calu-6 cells (American Type Culture Collection) derived from a human lung carcinoma were maintained in Dulbecco's modified Eagle medium with 1% sodium pyruvate (100 mM) and 1% nonessential amino acids. Each medium was supplemented with 10% fetal bovine serum, 2 mM L-glutamine, 100 units of penicillin per milliliter, and 100 mg of streptomycin per liter and incubated at 37°C in 5% carbon dioxide. LLC tumors were grown in male C57BL/6 mice, and Calu-6 tumors in male CD-1 nude mice (both mouse strains, ~20 g; Charles River U.K. Ltd.), by subcutaneous injection of 10^6 tumor cells into the inner right thigh (LLC) or interscapular region (Calu-6). Biodistribution and imaging studies were performed at days 15 and 25 after inoculation of LLC and Calu-6 tumor cells, respectively.

Biodistribution Studies

We first investigated the biodistribution of ^{18}F-AH111585 in mice bearing LLC tumors. Mice received 1.0 MBq of ^{18}F-AH111585 as an intravenous bolus via the tail vein and were humanely sacrificed at 5, 10, 30, 60, 120, and 240 min after injection. Blood, tumor, and major organs were collected, weighed, and counted in a γ-counter (Wallac Wizard; Perkin Elmer LAS Ltd.). The percentage of injected dose per gram (%ID/g) or percentage of injected dose (%ID) was determined for each sample.

Small-Animal PET and micro-CT Imaging of Calu-6 Tumor–Bearing Mice

Calu-6 tumor–bearing mice were used for small-animal PET imaging, which was performed on a microPET-P4 system (Siemens Inc.). Images were generated from 3-dimensional sinogram data, rebinned to 2-dimensional format by the Fourier rebinning algorithm, followed by 2-dimensional filtered backprojection. For imaging studies, the animal model described above was used, followed by injection of 5.0 MBq of ^{18}F-AH111585 as a bolus via the tail vein. Imaging was performed dynamically at 120 min after injection for 10 min, with the animal anesthetized via inhaled isoflurane. The microPET scanner was calibrated in terms of absolute activity concentration (kBq/cm^3) by imaging a phantom approximating the dimensions of a mouse body and filled with a known concentration of ^{18}F. Ten minutes before the beginning of the CT image acquisition, each mouse received an intravenous bolus of iohexol (0.1 mL) (Omnipaque; GE Healthcare) to improve tumor contrast. Imaging was performed using the microCAT II system (Siemens Inc.), with manufacturer-recommended settings—360° total rotation; 400-ms exposure time, with the camera set at 70 kVp with 500 μA; and binning set at 4 × 4, to give a resolution of 200 μm—giving a total radiation dose within safe exposure limits (*20*). Images were reconstructed using the image reconstruction, visualization, and analysis program supplied by the manufacturer. Small-animal PET and CT data were analyzed by using Amide software (http://amide.sourceforge.net). Imaging data are expressed as %ID/g.

Paclitaxel and ZD4190 Treatment

The effect of treatment on the tumor uptake of ^{18}F-AH111585 was investigated by submitting LLC tumor–bearing C57BL/6 mice

to paclitaxel therapy and Calu-6 tumor–bearing CD-1 nude mice to ZD4190 therapy. Intraperitoneal paclitaxel (Sigma Aldrich) therapy was initiated 7 d after LLC tumor induction, with the administration of paclitaxel. Paclitaxel was dissolved in dimethylsulfoxide and injected (100 μL) into mice ($n = 6$) at 5 or 10 mg/kg intraperitoneally. On the same days, control animals received an injection of vehicle alone that did not contain any paclitaxel. Paclitaxel was further administered on the subsequent 3 days (with appropriate vehicle control). Paclitaxel was well tolerated, with no significant effects on animal health observed. Groups were housed separately under the same conditions throughout. Five days after the final round of paclitaxel therapy, the mice received a coinjection of ^{18}F-AH111585 (1.0 MBq) and ^{14}C-FDG (1.0 MBq) (American Radiolabeled Chemicals, Inc.) and were sacrificed 120 min after injection. Tumors were dissected, weighed, and assayed for radioactivity.

ZD4190 was administered orally to mice bearing Calu-6 tumors inoculated 23 d before ZD4190 administration ($n = 10$) at 100 mg/kg after the day 0 baseline small-animal PET imaging and recovery from isoflurane anesthesia. Similarly, control animals ($n = 5$) received the vehicle alone. ZD4190 was administered again on 2 further consecutive days (with appropriate vehicle control). Groups were housed separately under the same conditions throughout. Two hours after the final dose of ZD4190 or vehicle control, animals were injected with an intravenous bolus of ^{18}F-AH111585 (5.0 MBq), housed individually in metabolism cages, and euthanized 120 min after injection. Each animal was then reimaged on the small-animal PET and micro-CT cameras. During the experimental period, tumor size was assessed via external caliper measurements. For both LLC and Calu-6 tumors, tumor size remained comparable ($P > 0.05$) over the duration of paclitaxel or ZD4190 treatment, respectively.

Microvascular Density (MVD) Measurement

Briefly, after the mice were euthanized, tumors were immediately excised and placed in a neutral buffered formalin or zinc fixative. After histologic processing, 4-μm slices from LLC tumors were analyzed for MVD, which was calculated as the highest MVD (h-MVD). For h-MVD, the 3 highest areas of vascularity across the whole tumor were selected on the basis of visual examination, and the numbers of angiogenic vessels were counted in each field of view. The h-MVD was selected and expressed as MVD/mm^2. The MVD of Calu-6 tumors was quantified using a different method from the one used to assess the LLC tumors, as described previously (*21*). Briefly, tumor specimens fixed in zinc fixative (PharMingen) were stained for CD31 using a chromagen endpoint and analyzed in a masked manner to treatment assignment using a KS400 instrument (Imaging Associates). MVD was calculated as the CD31-positive vessel number per 5,000-μm^2 viable tumor area in each tumor section.

Data Analysis

All experimental data were analyzed using an unpaired 2-tailed *t* test with software (GraphPad Prism, version 4.00 for Windows; GraphPad Software Inc.). *P* values of less than 0.05 were considered significant.

RESULTS

LLC Biodistribution Studies

Biodistribution data on ^{18}F-AH111585 in LLC tumor–bearing C57BL/6 mice are summarized in Table 1 and Figure 1.

In the LLC tumor model, ^{18}F-AH111585 has rapid tumor uptake (2.7 ± 0.53 %ID/g at 5 min after injection) and rapid background clearance (blood, skeletal muscle, lung, and liver assessed). Tumor uptake peaked 10 min after injection, with 3.1 ± 0.68 %ID/g. Retention within the tumor was 55% of the compound delivered 2 h after injection, with 1.49 ± 0.32 %ID/g of ^{18}F-AH111585 remaining. No retention was observed in any other organ. Baseline Calu-6 tumor uptake of ^{18}F-AH111585 was equivalent to that seen with the LLC (data not shown).

Figure 1B shows the LLC tumor–to–tissue ratios obtained over time with ^{18}F-AH111585. The data demonstrate that because of the rapid clearance characteristics of ^{18}F-AH111585 from the blood and other background tissues, biodistribution ratios above 1.5 (blood and muscle) were achieved 30 min after injection. Further improvements in the LLC tumor–to–key organ ratios were obtained by delaying dissection until 240 min after injection. As expected, the majority of activity (69.7 ± 3.6 %ID) was excreted via the kidneys and urine by 120 min, with 15.0 ± 2.6 %ID excreted via the gastrointestinal tract (Fig. 1C). The absence of an increase in gastrointestinal tract activity over time indicates that ^{18}F-AH111585 does not undergo significant biliary excretion.

Effect of Paclitaxel Therapy on ^{18}F-AH111585 Uptake

^{18}F-AH111585 was coinjected with ^{14}C-FDG to obtain a direct comparison between the 2 imaging agents in the same LLC tumor–bearing animal. The data demonstrate that the LLC uptake of ^{18}F-AH111585 was decreased from 1.71 ± 0.33 %ID/g to 1.17 ± 0.21 %ID/g for the 5 mg/kg group (not statistically significant at the $P = 0.082$ level using Student *t* test) and significantly decreased ($P < 0.05$) to 1.11 ± 0.11 %ID/g for the 10 mg/kg group (Fig. 2). In tumors of equivalent weight, this is a decrease in uptake of 35% at the highest dose level, compared with the control. The data for ^{14}C-FDG uptake demonstrate no change in uptake at the 5 and 10 mg/kg dose levels, compared with the control (5.12 ± 0.85 %ID/g, 5.45 ± 0.55 %ID/g, and 5.64 ± 1.32 %ID/g for control, 5 mg/kg, and 10 mg/kg groups, respectively). In paclitaxel-treated LLC tumors, h-MVD/mm^2 decreased nonsignificantly to 128 ± 24 and 111 ± 52 for the 5 and 10 mg/kg dose levels of paclitaxel, respectively, compared with the vehicle control–treated tumors (161 ± 107 h-MVD/mm^2).

Effect of ZD4190 Therapy on ^{18}F-AH111585 Uptake

Small-animal PET and micro-CT imaging data were acquired before and after 3 doses (100 mg/kg) of ZD4190 or the vehicle control. As can be seen in Figure 3, the uptake of ^{18}F-AH111585 in Calu-6 tumors was reduced significantly with 3 doses of ZD4190, with an average reduction in the %ID/g across the 10 animals examined of 31.8% ± 4.6% (calculated from imaging region-of-interest [ROI] data).

Skeletal muscle was used as a reference tissue for ROI analysis, and the data demonstrate that muscle uptake was maintained before and after therapy, indicating that the tumor decrease seen with ZD4190 therapy was specific. Compar-

TABLE 1. Biodistribution of ^{18}F-AH111585 in Mouse LLC Model

Time (min after injection)	Biodistribution (%ID/g)				
	Blood	Muscle	Lung	Liver	Tumor
5	6.35 (2.34)	1.78 (0.57)	6.54 (1.71)	6.01 (1.03)	2.69 (0.53)
10	6.56 (1.92)	1.66 (0.14)	8.20 (1.71)	5.43 (1.05)	3.11 (0.68)
30	1.81 (0.53)	1.03 (0.34)	3.90 (1.41)	2.57 (0.69)	2.68 (0.47)
60	0.84 (0.39)	0.56 (0.23)	2.12 (0.90)	1.48 (0.65)	1.84 (0.45)
120	0.45 (0.13)	0.27 (0.07)	1.17 (0.28)	0.89 (0.29)	1.49 (0.32)
240	0.07 (0.02)	0.05 (0.01)	0.27 (0.09)	0.17 (0.02)	0.40 (0.05)

Data are mean ± SD of %ID/g; $n = 6$ per time point.

ison with the vehicle control animals demonstrates that over the same 3-d dosing period, the Calu-6 tumor uptake of ^{18}F-AH111585 increased from the pre- to the posttreatment image, with an average increase of 26.9% ± 9.4%. Statistical analysis of the treated and control groups demonstrated a clear difference at the $P < 0.01$ level (determined via t test).

After the final imaging study, selected tissues were dissected, well counted, and assessed for MVD. These data demonstrated a reduced uptake of ^{18}F-AH111585 into Calu-6 tumors of 2.1 ± 0.1 %ID/g, compared with the vehicle control–treated Calu-6 tumor uptake of 2.4 ± 0.8 %ID/g (a decrease of 13%). MVD analysis of Calu-6 tumors demonstrated an equivalent ($P > 0.05$) level of vascularity after 3 doses of ZD4190 or vehicle control (0.06 ± 0.05 and 0.05 ± 0.04 MVD/5 mm^2, respectively). During the experimental period, tumor size was maintained in both the control and the ZD4190-treated groups.

Figure 4 shows representative fused small-animal PET and micro-CT images for ZD4190-treated and vehicle control animals. The before and after images show decreased ^{18}F-AH111585 uptake (with ZD4190 therapy) and increased ^{18}F-AH111585 uptake (with vehicle control) before and after therapy.

DISCUSSION

Previously, quantification of tumor vasculature has been assessed in surgical specimens or preclinical samples using immunohistochemistry. However, such assays are impractical in clinical trials not only because of potential variability in the measurement of MVD (depending on the choice of marker [e.g., CD31 or CD105] or endpoint [e.g., Chalkey counts, whole-tumor image analysis, or hot-spot analysis] (*16*)) but also because of the ethical and physical limitations of serial invasive procedures. In addition, the inherent anatomic and physiologic heterogeneity of tumors, which is likely to require that multiple samples be taken at any given time (*22*), make such assays impractical in clinical trials. Clearly, a noninvasive method for assessing tumor vascularity could obviate these technical challenges.

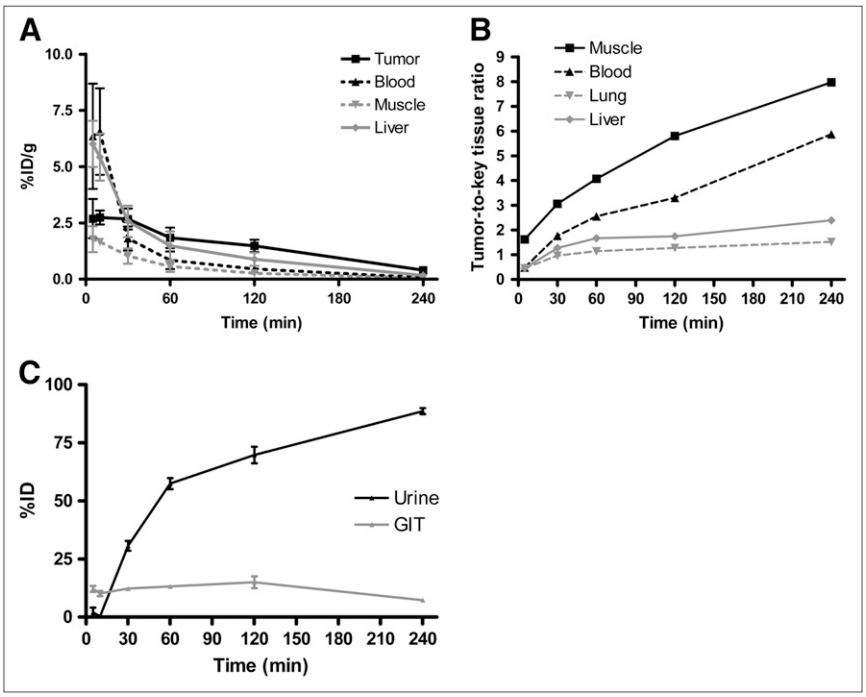

FIGURE 1. (A) Biodistribution and clearance profile of ^{18}F-AH111585. (B) Key tumor–to–background-tissue ratios of ^{18}F-AH111585; values are expressed as ratio of tumor %ID/g to background tissue %ID/g. (C) Excretion profile of ^{18}F-AH111585 in mouse LLC model up to 240 min after injection. Values are expressed as %ID/g or %ID and presented as mean (±SD) of 5 experiments ($n = 6$).

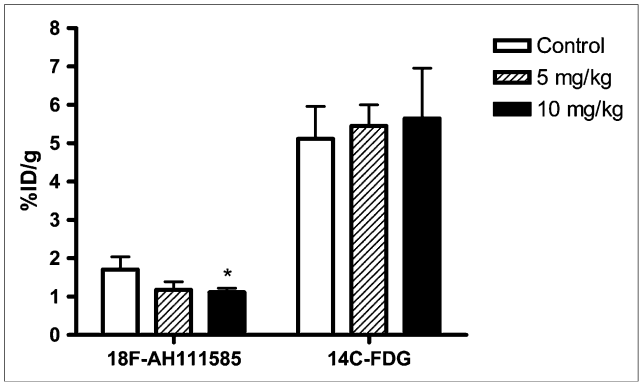

FIGURE 2. Inhibition of ^{18}F-AH111585 uptake by low-dose paclitaxel (5 and 10 mg/kg) therapy in the mouse LLC model (120 min after injection of ^{18}F-AH111585, day 15 after LLC cell inoculation). At the same paclitaxel dose level, no effect was observed on ^{14}C-FDG uptake. Values are expressed in %ID/g and presented as mean (±SD) of 2 experiments ($n = 4$). *$P <$ 0.05, compared with the corresponding control group.

In this study, we present a preclinical assessment of a novel cyclic RGD-based radioligand for $\alpha_v\beta_3/\alpha_v\beta_5$, ^{18}F-AH111585, an analog of a peptide pharmacophore isolated from a phage-display library (*23*). The original peptide sequence (RGD-4C) was optimized extensively to improve

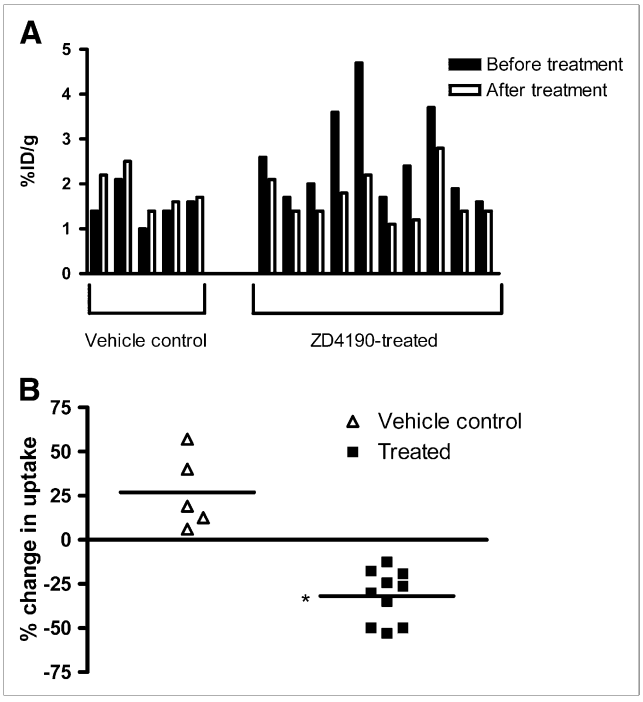

FIGURE 3. (A) Inhibition of ^{18}F-AH111585 uptake in Calu-6 tumors in nude mice before and after treatment with 3 doses of ZD4190 (100 mg/kg) or vehicle control. Values are expressed in %ID/g and presented as individual data. (B) Summarized data demonstrate percentage change in uptake of ^{18}F-AH111585 in Calu-6–tumored CD-1 nude mice before and after treatment with 3 doses of ZD4190 (100 mg/kg) or vehicle control. Data are presented for individual animals. *$P <$ 0.01, compared with vehicle control group.

in vivo stability and increase plasma half-life (*18*) while maintaining high affinity for $\alpha_v\beta_3/\alpha_v\beta_5$: the observed K_i for the cold compound (AH111585) was calculated to be 10.2 nM in competition with radioactive ^{125}I-echistatin, an RGD-containing peptide isolated from snake venom.

Biodistribution studies for ^{18}F-AH111585 revealed favorable in vivo pharmacokinetic properties, with significant levels of receptor-specific tumor uptake determined via cold-peptide blocking studies (data not shown). In addition, imaging results demonstrated high contrast visualization of Calu-6 tumors, both with and without ZD4190 therapy. Although several groups have developed radiolabeled RGD compounds that have shown promise in terms of tumor uptake and tumor-to-background ratios (*12,24,25*), relatively little attention has been focused on the ability of these radiotracers to monitor the response of tumors to therapies that target the vasculature, the most likely clinical use of these imaging agents. One exception is the work by Jung et al. (*26*), who have demonstrated that paclitaxel therapy (an antimicrotubule agent commonly used in the treatment of breast and non–small cell lung cancer (*27*)) resulted in a decreased LLC uptake of a ^{99m}Tc-labeled glucosamino RGD-containing peptide. The authors stated that these data support the use of the radiolabeled RGD peptide for monitoring response to antiangiogenic therapy. In our study, paclitaxel was used at lower doses than those used by Jung et al.; animals were dosed at 5 and 10 mg/kg. At these low doses, paclitaxel is reported to cause an antiangiogenic effect without significant tumor shrinkage (*28*). Our data show that ^{18}F-AH111585 detects changes in the level of tumor angiogenesis as determined by MVD analysis.

We coinjected ^{14}C-FDG with ^{18}F-AH111585 after paclitaxel therapy to compare data with the results of ^{18}F-AH111585 alone and generate data with an imaging agent radiolabeled with ^{18}F that is used extensively in the clinic for tumor imaging (*29*). ^{18}F-AH111585 tumor uptake was more sensitive to paclitaxel therapy, because a reduction in uptake was seen, whereas ^{14}C-FDG uptake remained unchanged. The reduction in ^{18}F-AH111585 uptake was matched by a decrease in the tumor h-MVD: with low-dose paclitaxel, a 20% decrease in MVD was detected when compared with a separate group of vehicle control–treated LLC tumors. This finding demonstrates that ^{18}F-AH111585 is able to detect vascular changes that occur through the use of paclitaxel.

That ^{18}F-AH111585 is able to target neovasculature via the $\alpha_v\beta_3/\alpha_v\beta_5$ receptors expressed on endothelial cells is supported by the work of Pasqualini et al., who demonstrated that tumor vessels were the structural elements most targeted by the RGD sequence (*30*). However, the predominantly high expression of integrins on endothelial cells, compared with tumor cells, is not necessarily a feature of all tumors; metastatic melanoma, for instance, has high expression of the receptor. In a study by Beer et al., who imaged melanoma by ^{18}F-galacto-RGD, expression of the $\alpha_v\beta_3$ integrin was higher on tumor cells than on tumor vasculature (*31*). This high $\alpha_v\beta_3$ expression on tumor cell lines has also been confirmed pre-

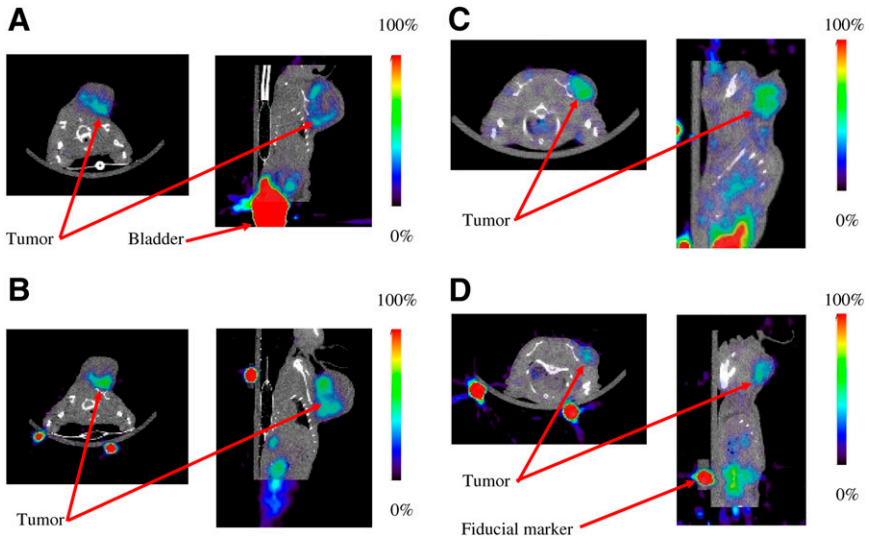

FIGURE 4. Representative coregistered small-animal PET and micro-CT images demonstrating ^{18}F-AH111585 uptake at 120 min in Calu-6 xenograft model before (A) and after (B) administration of 3 doses of vehicle control or before (C) and after (D) 3 doses of ZD4190 (100 mg/kg). Contrast is clearly seen in Calu-6 tumors located on left shoulder region in both ZD4190-treated and vehicle control animals. The only additional higher activity concentration was found in bladder. In addition, ^{22}Na fiducial markers can be seen located on base of imaging bed (used for PET/CT coregistration). ROI analysis for tumor uptake before ZD4190 therapy was 1.7 %ID/g, decreasing to 1.1 %ID/g after ZD4190 therapy. Muscle uptake was maintained at 0.5 %ID/g in pre- and post-ZD4190–therapy images. For animals treated with vehicle control alone, ROI analysis for tumor uptake before vehicle control was 2.1 %ID/g, increasing to 2.5 %ID/g after therapy. Muscle uptake was maintained at 0.3 %ID/g in pre- and posttherapy images.

clinically, using tumor cell lines such as melanoma (M21) and glioblastomas (U87MG) (*32*). However, the LLC and Calu-6 cells used in the studies reported here are known to have low $\alpha_v\beta_3$ expression, as determined by in vitro binding studies (*26*) for LLC and by fluorescence-activated cell sorter analysis (data not shown) for both LLC and Calu-6 cells. Therefore, we can speculate that the uptake of ^{18}F-AH111585 seen in vivo in these models is predominately related to endothelial cell $\alpha_v\beta_3$ and $\alpha_v\beta_5$ expression.

However, a potential limitation of targeting $\alpha_v\beta_3$ and $\alpha_v\beta_5$ integrins is that the distinction between tumors and inflammation might be impaired. For example, it has been reported that in patients with pigmented villonodular synovitis the uptake of ^{18}F-galacto-RGD in inflammatory lesions can be intense and similar to the uptake observed in malignancies (*33*). This might be a shortcoming of ours and others' approaches with RGD-based tracers, which, like ^{18}F-FDG, can show high uptake in inflammatory cells (*34*).

Calu-6 small-animal PET images showed high activity in the bladder, indicating that ^{18}F-AH111585 is excreted mainly via the kidneys into the urine. Biodistribution data confirmed this finding, with greater than 75 %ID being excreted via the urine 4 h after injection of ^{18}F-AH111585.

MVD analysis of Calu-6 tumors at the end of study demonstrated an equivalent level of vascularity after 3 doses of ZD4190 or vehicle control, which is consistent with the equivalent uptake of ^{18}F-AH111585 after treatment in ZD4190 and control groups. This equivalence may be due, in part, to the higher initial uptake of ^{18}F-AH111585 in several tumors in the ZD4190 group than in the control group. When intraanimal pre- and posttreatment values were analyzed, a significant reduction (32%; $P < 0.01$) in ^{18}F-AH111585 uptake was evident in Calu-6 tumors from mice treated for 3 d with ZD4190. In contrast, a 27% increase in ^{18}F-AH111585 uptake ($P < 0.01$) was observed in Calu-6 tumors from animals treated with vehicle over the same period. This change in uptake is consistent with the activity of ZD4190 against VEGFR-2 tyrosine kinase; other inhibitors of this receptor tyrosine kinase have been shown to reduce tumor vascular density after relatively acute treatment (*35*).

These data demonstrate the value of longitudinal PET, because the uptake of ^{18}F-AH111585 can be easily followed over time in individual animals before and after therapy, in contrast to MVD analysis (*16*).

CONCLUSION

The data presented in this article demonstrate that ^{18}F-AH111585 is a promising ^{18}F-labeled RGD tracer, with favorable biodistribution properties that allow the noninvasive assessment of tumor vascularity and response to treatments that affect the tumor vascular compartment. Preliminary clinical studies with ^{18}F-AH111585 have already proven that this radioligand has a suitable biodistribution and dosimetry profile (*36*) and can successfully image metastatic breast cancer lesions (*7*): 7 patients with a total of 18 tumors detectable on CT were imaged with ^{18}F-AH111585 PET, and all tumors were visible.

Consequently, this agent may be used to quantify tumor vasculature and, when used alone or in combination with additional functional imaging modalities, should enhance our mechanistic understanding of how novel therapeutic strategies impact on tumors.

ACKNOWLEDGMENTS

We thank Colin Steel and the cyclotron operators of Hammersmith Imanet Ltd. for providing us with ^{18}F, Maria

Constantinou for supplying ^{18}F-AH111585, and Julian Goggi for helping with image analysis. We also thank Lyndsey Hanson and Alison Bigley for performing CD31 analysis in Calu-6 tumors.

REFERENCES

1. Folkman J. Angiogenesis: an organizing principle for drug discovery? *Nat Rev Drug Discov.* 2007;6:273–286.
2. Hinnen P, Eskens FA. Vascular disrupting agents in clinical development. *Br J Cancer.* 2007;96:1159–1165.
3. Munoz R, Shaked Y, Bertolini F, Emmenegger U, Man S, Kerbel RS. Anti-angiogenic treatment of breast cancer using metronomic low-dose chemotherapy. *Breast.* 2005;14:466–479.
4. Bradley DP, Tessier JL, Checkley D, et al. Effects of AZD2171 and vandetanib (ZD6474, Zactima) on haemodynamic variables in an SW620 human colon tumour model: an investigation using dynamic contrast-enhanced MRI and the rapid clearance blood pool contrast agent, P792 (gadomelitol). *NMR Biomed.* 2008;21:42–52.
5. Daldrup-Link HE, Simon GH, Brasch RC. Imaging of tumor angiogenesis: current approaches and future prospects. *Curr Pharm Des.* 2006;12:2661–2672.
6. McDonald DM, Teicher BA, Stetler-Stevenson W, et al. Report from the Society for Biological Therapy and Vascular Biology faculty of the NCI Workshop on Angiogenesis Monitoring. *J Immunother.* 2004;27:161–175.
7. Kenny LM, Coombes CR, Oulie I, et al. Phase I trial of the positron-emitting Arg-Gly-Asp (RGD) peptide radioligand ^{18}F-AH111585 in breast cancer patients. *J Nucl Med.* 2008;49:879–886.
8. Horton MA. The αvβ3 integrin "vitronectin receptor." *Int J Biochem Cell Biol.* 1997;29:721–725.
9. Hynes RO. Integrins: versatility, modulation, and signaling in cell adhesion. *Cell.* 1992;69:11–25.
10. Eliceiri BP, Cheresh DA. The role of αv integrins during angiogenesis: insights into potential mechanisms of action and clinical development. *J Clin Invest.* 1999;103:1227–1230.
11. Brooks PC, Montgomery AM, Rosenfeld M, et al. Integrin $\alpha_v\beta_3$ antagonists promote tumor regression by inducing apoptosis of angiogenic blood vessels. *Cell.* 1994;79:1157–1164.
12. Beer AJ, Niemeyer M, Carlsen J, et al. Patterns of $\alpha_v\beta_3$ expression in primary and metastatic human breast cancer as shown by ^{18}F-galacto-RGD PET. *J Nucl Med.* 2008;49:255–259.
13. Chen X, Tohme M, Park R, Hou Y, Bading JR, Conti PS. Micro-PET imaging of $\alpha_v\beta_3$-integrin expression with ^{18}F-labeled dimeric RGD peptide. *Mol Imaging.* 2004;3:96–104.
14. Haubner RH, Wester HJ, Weber WA, Schwaiger M. Radiotracer-based strategies to image angiogenesis. *Q J Nucl Med.* 2003;47:189–199.
15. Hahnfeldt P, Panigrahy D, Folkman J, Hlatky L. Tumor development under angiogenic signaling: a dynamical theory of tumor growth, treatment response, and postvascular dormancy. *Cancer Res.* 1999;59:4770–4775.
16. Hlatky L, Hahnfeldt P, Folkman J. Clinical application of antiangiogenic therapy: microvessel density, what it does and doesn't tell us. *J Natl Cancer Inst.* 2002;94:883–893.
17. Wedge SR, Ogilvie DJ, Dukes M, et al. ZD4190: an orally active inhibitor of vascular endothelial growth factor signaling with broad-spectrum antitumor efficacy. *Cancer Res.* 2000;60:970–975.
18. Indrevoll B, Kindberg GM, Solbakken M, et al. NC-100717: a versatile RGD peptide scaffold for angiogenesis imaging. *Bioorg Med Chem Lett.* 2006;16:6190–6193.
19. Glaser M, Morrison M, Solbakken M, et al. Radiosynthesis and biodistribution of cyclic RGD peptides conjugated with novel [^{18}F]fluorinated aldehyde-containing prosthetic groups. *Bioconjug Chem.* 2008;19:951–957.
20. Obenaus A, Smith A. Radiation dose in rodent tissues during micro-CT imaging. *J XRay Sci Technol.* 2004;12:241–249.
21. Wedge SR, Kendrew J, Hennequin LF, et al. AZD2171: a highly potent, orally bioavailable, vascular endothelial growth factor receptor-2 tyrosine kinase inhibitor for the treatment of cancer. *Cancer Res.* 2005;65:4389–4400.
22. Gerber HP, Ferrara N. Pharmacology and pharmacodynamics of bevacizumab as monotherapy or in combination with cytotoxic therapy in preclinical studies. *Cancer Res.* 2005;65:671–680.
23. Pasqualini R, Koivunen E, Ruoslahti E. A peptide isolated from phage display libraries is a structural and functional mimic of an RGD-binding site on integrins. *J Cell Biol.* 1995;130:1189–1196.
24. Haubner R. $\alpha_v\beta_3$-integrin imaging: a new approach to characterise angiogenesis? *Eur J Nucl Med Mol Imaging.* 2006;33(suppl 1):54–63.
25. Liu S, Hsieh WY, Jiang Y, et al. Evaluation of a ^{99m}Tc-labeled cyclic RGD tetramer for noninvasive imaging integrin $\alpha_v\beta_3$-positive breast cancer. *Bioconjug Chem.* 2007;18:438–446.
26. Jung KH, Lee KH, Paik JY, et al. Favorable biokinetic and tumor-targeting properties of ^{99m}Tc-labeled glucosamino RGD and effect of paclitaxel therapy. *J Nucl Med.* 2006;47:2000–2007.
27. Horwitz SB. Taxol (paclitaxel): mechanisms of action. *Ann Oncol.* 1994;5(suppl 6):S3–S6.
28. Lau DH, Xue L, Young LJ, Burke PA, Cheung AT. Paclitaxel (Taxol): an inhibitor of angiogenesis in a highly vascularized transgenic breast cancer. *Cancer Biother Radiopharm.* 1999;14:31–36.
29. Juweid ME. Utility of positron emission tomography (PET) scanning in managing patients with Hodgkin lymphoma. *Hematology Am Soc Hematol Educ Program.* 2006:259–265, 510–511.
30. Pasqualini R, Koivunen E, Ruoslahti E. αv integrins as receptors for tumor targeting by circulating ligands. *Nat Biotechnol.* 1997;15:542–546.
31. Beer AJ, Haubner R, Sarbia M, et al. Positron emission tomography using [^{18}F]galacto-RGD identifies the level of integrin $\alpha_v\beta_3$ expression in man. *Clin Cancer Res.* 2006;12:3942–3949.
32. Haubner R, Wester HJ, Weber WA, et al. Noninvasive imaging of $\alpha_v\beta_3$ integrin expression using ^{18}F-labeled RGD-containing glycopeptide and positron emission tomography. *Cancer Res.* 2001;61:1781–1785.
33. Haubner R, Weber WA, Beer AJ, et al. Noninvasive visualization of the activated alphavbeta3 integrin in cancer patients by positron emission tomography and [^{18}F]galacto-RGD. *PLoS Med.* 2005;2:e70.
34. Kubota R, Yamada S, Kubota K, Ishiwata K, Tamahashi N, Ido T. Intratumoral distribution of fluorine-18-fluorodeoxyglucose in vivo: high accumulation in macrophages and granulation tissues studied by microautoradiography. *J Nucl Med.* 1992;33:1972–1980.
35. Smith NR, James NH, Oakley I, et al. Acute pharmacodynamic and antivascular effects of the vascular endothelial growth factor signaling inhibitor AZD2171 in Calu-6 human lung tumor xenografts. *Mol Cancer Ther.* 2007;6:2198–2208.
36. McParland BJ, Miller MP, Spinks TJ, et al. The biodistribution and radiation dosimetry of the Arg-Gly-Asp peptide ^{18}F-AH111585 in healthy volunteers. *J Nucl Med.* 2008;49:1664–1667.